.

RESOLUTION AND STABILITY ANALYSIS IN LINEARIZED CONDUCTIVITY AND WAVE IMAGING. PART I: FULL APERTURE CASE

HABIB AMMARI, JOSSELIN GARNIER, AND KNUT SØLNA

ABSTRACT. In this paper we consider resolution estimates in both the linearized conductivity problem and the wave imaging problem. Our purpose is to provide explicit formulas for the resolving power of the measurements in the presence of measurement noise. We show that the low-frequency regime in wave imaging as well as the inverse conductivity problem are very sensitive to measurement noise while high-frequencies increase stability in wave imaging.

1. INTRODUCTION

The main objective of this paper is to introduce the notion of resolution in solving the inverse conductivity problem. We discuss resolution estimates in the case of conductivity data, and we contrast this process with resolution estimates based on Helmholtz data. In our analysis we moreover make use of asymptotic characterization of the measurements to get explicit results on their resolving power. For both the conductivity and the wave problems, we consider the imaging of a perturbed disk. For the conductivity problem, the data are collected on the boundary of a background medium containing the perturbed disk while for the Helmholtz equation, they consist of multi-static measurements on coincident transmitter and receiver arrays. The Born approximation is used in the wave propagation problem.

For the linearized conductivity problem, we first show that on the one hand, we have "infinite resolution" in the near-field limit and on the other hand, the relative resolution decreases rapidly with "depth" (the depth increases when the radius of the inclusion decreases). We also give conditions on the signal-to-noise ratio (SNR) and the radius of the inclusion in order to resolve the pth Fourier mode of the perturbation and explicitly answer the question: for a fixed SNR and radius of the unperturbed disk which modes can be resolved? We finally characterize the smallest radius one can probe for a certain mode number p and a given SNR and show that the linearized inverse conductivity problem is very sensitive to noise.

For the wave imaging problem under the Born approximation, we consider two regimes: a high-frequency regime where the radius of the inclusion is much larger than the wavelength and a low-frequency regime where it is smaller. We first show that in the high-frequency regime the resolution estimates are relatively insensitive to noise for modes that correspond to lengths larger than half a wavelength. High-frequencies increase stability. On the other hand, the low-frequency regime is, as the conductivity case, very sensitive to noise. We provide explicit formulas for the modes that can be estimated for a given SNR and radius of the inclusion.

2000 *Mathematics Subject Classification.* 35R30, 35B30.
Key words and phrases. Inverse conductivity problem, wave imaging, resolution, stability.
This work was supported by the ERC Advanced Grant Project MULTIMOD–267184.

In connection with our results, we refer in particular to the recent works by Isakov [19] and Nagayasu-Uhlmann-Wang [20]. For further discussions on resolution for conductivity and wave imaging, see [6, 8, 9, 10, 11, 12, 13, 15, 18]. In [19], an evidence of increasing stability in wave imaging when frequency is growing was given. In [20], a stability estimate for a linearized conductivity problem was derived. Our results in this paper confirm these important observations and quantify them precisely in terms of the SNR. As far as we know, our formulas for the resolving power of the measurements in the presence of measurement noise are new. They provide a deep understanding of the ill-posed nature of the considered imaging problems and clarify the connection between the inverse conductivity problems and the wave imaging problems. We emphasize that the conclusions of this paper hold only under the assumption that the noise is in the measurements and not in the medium. For medium noise, the whole picture is quite different. This would be the subject of a forthcoming investigation. We will also consider consider the limited-view case. Another challenging problem is to extend the present resolution analysis to static and dynamic elasticity. In view of [2] similar resolution estimations may be expected to hold in the elastic case.

2. Interface Estimation with Conductivity Data

In this section we discuss estimation in the case of conductivity data in the two-dimensional case. We will contrast this process with estimation based on Helmholtz data in Section 3.

2.1. **Differential Measurements.**

The measurements are taken on a circle of unit radius in our non-dimensionalized setting. The domain of interest, encapsulated by the measurements, is thus

$$\Omega = \left\{ \boldsymbol{x} = r\boldsymbol{e}_\theta \mid r \leq 1,\, 0 \leq \theta < 2\pi \right\} , \tag{1}$$

where $\boldsymbol{e}_\theta = (\cos\theta, \sin\theta)$. Imbedded in the domain there is a homogeneous inclusion centered at the origin and with the shape of a perturbed circle. Our objective is to estimate the rim of the inclusion. We denote the domain of the unperturbed disk by D and the perturbed domain by D_ε:

$$D = \left\{ \boldsymbol{x} = r\boldsymbol{e}_\theta \mid r \leq \alpha,\, 0 \leq \theta < 2\pi \right\} , \tag{2}$$

$$D_\varepsilon = \left\{ \boldsymbol{x} = r\boldsymbol{e}_\theta \mid r \leq \alpha + \varepsilon h(\theta),\, 0 \leq \theta < 2\pi \right\} . \tag{3}$$

We let here h be order one and assume that h is of class $\mathcal{C}^1$ and $\varepsilon \ll 1$.

The field for different source configurations are indexed by $m = \pm 1, \pm 2, \cdots$ and chosen to solve in the perturbed case:

$$\nabla \cdot (1 + (k-1)\chi_{D_\varepsilon}) \nabla u_\varepsilon^m = 0 \, , \qquad \boldsymbol{x} \in \Omega \, , \tag{4}$$

with the Neumann boundary conditions at the surface $\partial\Omega$:

$$\frac{\partial u_\varepsilon^m}{\partial \nu}(\boldsymbol{e}_\theta) = e^{-im\theta} \, , \qquad \theta \in [0, 2\pi) \, , \qquad\qquad \int_0^{2\pi} u_\varepsilon^m(\boldsymbol{e}_\theta) d\theta = 0 \, . \tag{5}$$

Here, ν denotes the outward normal to $\partial\Omega$ and k is the contrast in the conductivity between the inclusion and the background. The field corresponding to the *unperturbed* domain D is denoted by $u^m = u_0^m$. The differential measurements are denoted by

$$\hat{a}_{n,m} = \int_0^{2\pi} e^{-in\theta}(u_\varepsilon^m - u^m)(\boldsymbol{e}_\theta)d\theta \,. \tag{6}$$

A central point of our analysis is to assess the resolving power of the measurements in the presence of measurement or instrument noise. We thus introduce

$$\hat{a}^{\text{meas}}_{n,m} = \hat{a}_{n,m} + \sigma \hat{W}_{n,m} \,, \tag{7}$$

with the noise terms $\hat{W}_{n,m}$ modeled as independent standard complex circularly symmetric Gaussian random variables (such that $\mathbb{E}[|\hat{W}_{m,n}|^2] = 1$) and σ thus modeling the noise magnitude.

In our analysis we moreover make use of asymptotic characterization of the wave field to get explicit results on the resolving power of the measurements. This representation uses the results of [5]. In fact, for any $|n|, |m| \ll (1/\epsilon)$, we have the representation

$$\hat{a}_{n,m} = (\mathcal{Q}\hat{h})_{n,m} + \varepsilon^2 \hat{V}_{n,m} \,, \tag{8}$$

where

$$(\mathcal{Q}\hat{h})_{n,m} = \varepsilon c_{n,m}(\alpha, k)\hat{h}_{n+m} \,, \tag{9}$$

with the coefficients

$$c_{n,m}(\alpha,k) = -\frac{8\pi(k - \text{sign}(nm))}{\alpha(k-1)} \frac{1}{(\alpha^{-|n|}\frac{k+1}{k-1} + \alpha^{|n|})(\alpha^{-|m|}\frac{k+1}{k-1} + \alpha^{|m|})} \,, \tag{10}$$

if $nm \neq 0$, and $c_{n,m}(\alpha, k) = 0$ if $nm = 0$. Here we have used the Fourier convention

$$\hat{h}_p = \frac{1}{2\pi}\int_0^{2\pi} h(\theta)e^{-ip\theta}d\theta \,, \qquad h(\theta) = \sum_{p=-\infty}^{\infty} \hat{h}_p e^{ip\theta} \,. \tag{11}$$

Thus, we have

$$\hat{a}^{\text{meas}}_{n,m} = (\mathcal{Q}\hat{h})_{n,m} + \sigma \hat{W}_{n,m} + \varepsilon^2 \hat{V}_{n,m} \,. \tag{12}$$

Note that $(\mathcal{Q}\hat{h})_{n,m} = (\mathcal{Q}\hat{h})_{m,n}$ and $(\mathcal{Q}\hat{h})_{n,-m} = (\mathcal{Q}\hat{h})_{-n,m}$.

2.2. **Short Range Sharp Resolving Power of Conductivity.** Our objective is now to identify the rim or perimeter perturbation of the inclusion, that is the function h. Note that, from (8), only $\hat{h}_p$ for $0 < |p| \ll 1/\varepsilon$ can be reconstructed from boundary measurements. Therefore, let $M \ll 1/\varepsilon$ be a positive integer and suppose that $\hat{h}_p = 0$ for $|p| \geq M$.

The adjoint of the operator $\mathcal{Q}$ defined by (9) is

$$(\mathcal{Q}^\star \hat{a})_p = \varepsilon \sum_{j=-\infty}^{\infty} \overline{c_{p-j,j}(\alpha,k)}\hat{a}_{p-j,j} \,. \tag{13}$$

We moreover have

$$(\mathcal{Q}^\star\mathcal{Q}\hat{h})_p = \varepsilon^2 q_p(\alpha,k)\hat{h}_p \,, \qquad q_p(\alpha,k) = \sum_{j=-\infty}^{\infty} |c_{p-j,j}(\alpha,k)|^2 \,. \tag{14}$$

The least squares estimate of $\hat{h}_p$ using $\hat{a}^{\rm meas}$ is

$$\begin{aligned}\hat{h}_p^{\rm est} &= \big((\mathcal{Q}^*\mathcal{Q})^{-1}\mathcal{Q}^*\hat{a}^{\rm meas}\big)_p = \varepsilon^{-2}q_p(\alpha,k)^{-1}\left(\mathcal{Q}^*\hat{a}^{\rm meas}\right)_p \\ &= \hat{h}_p + \varepsilon^{-2}q_p(\alpha,k)^{-1}\Big(\mathcal{Q}^*(\sigma\hat{W}+\varepsilon^2\hat{V})\Big)_p\,. \end{aligned} \tag{15}$$

We then have

$$\mathbb{E}\Big[\big|\hat{h}_p^{\rm est}-\hat{h}_p\big|^2\Big] \leq q_p(\alpha,k)^{-1}\bigg[\Big(\frac{\sigma}{\varepsilon}\Big)^2+\varepsilon^2\sum_{j=-\infty}^{\infty}|\hat{V}_{p-j,j}|^2\bigg], \tag{16}$$

using that

$$\mathbb{E}\Big[\big|(\mathcal{Q}^*\hat{W})_p\big|^2\Big] = \varepsilon^2 q_p(\alpha,k)\,,$$

and

$$\big|(\mathcal{Q}^*\hat{V})_p\big|^2 \leq \varepsilon^2 q_p(\alpha,k)\sum_{j=-\infty}^{\infty}|\hat{V}_{p-j,j}|^2\,.$$

We assume here

Assumption 1. $\varepsilon^2 \ll \sigma$.

Assumption 1 insures that indeed the instrument errors dominate the approximation error. We remark that we below assume without loss of generality that $p \geq 1$. We can therefore conclude from (16) that to resolve the pth mode of h, $\hat{h}_p$, we need the following resolving condition to be satisfied:

$$\Big(\frac{\sigma}{\varepsilon}\Big)^2 < q_p(\alpha,k)\,, \tag{17}$$

assuming that indeed $\hat{h}_p$ is of order one.

By substituting into (14) the following lower and upper bounds for $c_{n,m}(\alpha,k)$

$$\Big(\frac{8\pi(k-1)^2}{4\alpha(k+1)^2}\Big)\alpha^{|n|+|m|} \leq |c_{n,m}(\alpha,k)| \leq \Big(\frac{8\pi|k-1|}{\alpha(k+1)}\Big)\alpha^{|n|+|m|}\,, \tag{18}$$

we find that

$$\Big(\frac{8\pi(k-1)^2}{4(k+1)^2}\Big)^2 \leq \frac{q_p(\alpha,k)}{\alpha^{2p-2}\big(\frac{2\alpha^4}{1-\alpha^4}+p-1\big)} \leq \Big(\frac{8\pi(k-1)}{(k+1)}\Big)^2. \tag{19}$$

We introduce the signal to noise ratio SNR and the contrast adjusted signal to noise ratio SNR_k:

$$\mathrm{SNR} = \Big(\frac{\varepsilon}{\sigma}\Big)^2\,, \qquad \mathrm{SNR}_k = \frac{4\pi^2(k-1)^4}{(k+1)^4}\mathrm{SNR}\,. \tag{20}$$

The mode resolving sufficient condition is therefore:

$$\mathrm{SNR}_k^{-1} < \alpha^{2p-2}\Big(\frac{2\alpha^4}{1-\alpha^4}+p-1\Big)\,. \tag{21}$$

We can see that we have "infinite resolution" in the limit $\alpha \uparrow 1$ in the sense that we can estimate all modes $\hat{h}_p$ in this limit. We correspondingly have the following necessary condition associated with the lower bound in (19):

$$\widetilde{\mathrm{SNR}}_k^{-1} < \alpha^{2p-2}\Big(\frac{2\alpha^4}{1-\alpha^4}+p-1\Big)\,, \tag{22}$$

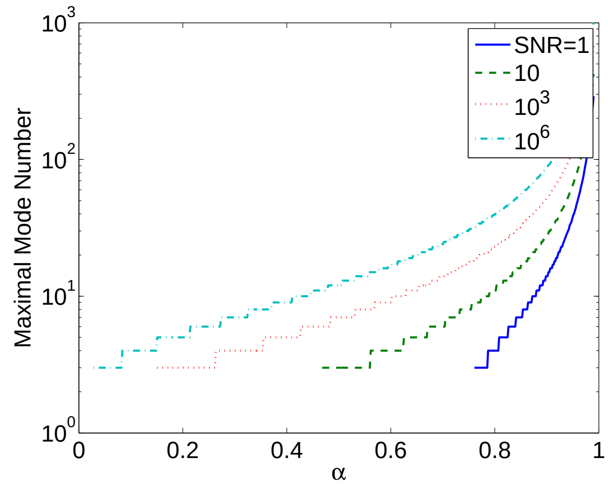

FIGURE 1. Maximal mode number $p(\alpha, \mathrm{SNR}_k)$ (see (24)) as function of radius α and signal to noise ratio SNR_k.

for

$$\widetilde{\mathrm{SNR}}_k = \frac{64\pi^2(k-1)^2}{(k+1)^2}\mathrm{SNR}\,, \tag{23}$$

which has exactly the same behavior as the sufficient condition (21). Therefore we will now only work with (21).

We can now answer the question: for a fixed SNR and radius α which modes can be resolved? From the previous analysis the answer is that it is possible to estimate the pth mode up to $p = p(\alpha, \mathrm{SNR}_k)$, where $p(\alpha, \mathrm{SNR}_k)$ is the resolving mode number bound defined by

$$p(\alpha, \mathrm{SNR}_k) = \sup\left\{ p \geq 1 \,\middle|\, \inf_{1\leq p' \leq p} \alpha^{2p'-2}\Big(\frac{2\alpha^4}{1-\alpha^4} + p' - 1\Big) > \mathrm{SNR}_k^{-1} \right\}. \tag{24}$$

If the set in the sup is empty, then $p(\alpha, \mathrm{SNR}_k) = 0$, which means that estimation is not possible. In Figure 1 we show the maximal mode number $p(\alpha, \mathrm{SNR}_k)$. It is seen that the relative resolution decreases rapidly with "depth" (decreasing radius α). Figure 2 shows the resolution bound as defined by

$$\lambda(\alpha, \mathrm{SNR}_k) = 2\pi\frac{\alpha}{p(\alpha, \mathrm{SNR}_k)}\,. \tag{25}$$

We remark that the resolution measured in this way actually improves for very small radius due to reduction in scale for fixed p with reduced radius. In fact, for large SNR_k, the function $\alpha \to \lambda(\alpha, \mathrm{SNR}_k)$ is approximately $-4\pi\alpha\ln(\alpha)/\ln(\mathrm{SNR}_k)$, it has a maximum whose value is $4\pi/(e\ln(\mathrm{SNR}_k))$ for the argument $\alpha = e^{-1}$. We will revisit this observation in the next subsection.

2.3. Probing in Depth with Conductivity.

We now revisit the question addressed in the previous subsection by considering the alternative question: for a fixed SNR and mode p, what is the minimal radius α of the inclusion that can be

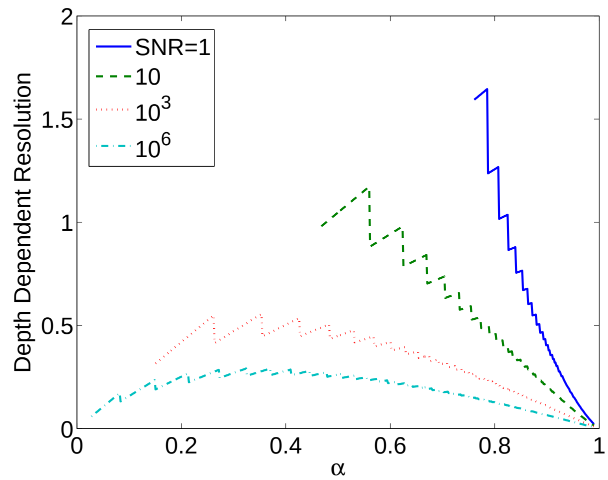

FIGURE 2. Resolution $\lambda(\alpha, \mathrm{SNR}_k)$ (see (25)) as function of radius α and signal to noise ratio SNR_k.

probed? We find from (21) that a resolving condition is $\alpha \geq \alpha^\star(p, \mathrm{SNR}_k)$ where we have defined the "resolving radius" by

$$\alpha^\star(p, \mathrm{SNR}_k) = \mathcal{F}_p^{-1}\Big(\frac{1}{\mathrm{SNR}_k}\Big) . \tag{26}$$

Here $\mathcal{F}_p^{-1}$ is the inverse of the function $\alpha \to \mathcal{F}_p(\alpha) = \alpha^{2p-2}\big(\frac{2\alpha^4}{1-\alpha^4} + p - 1\big)$ that is increasing and one-to-one from $[0, 1)$ to $[0, \infty)$. The quantity $\alpha^\star(p, \mathrm{SNR}_k)$ has the interpretation of being the smallest radius one can probe for a certain mode number p and signal to noise ratio SNR_k. The probing depth is of course limited by SNR_k. By reducing the mode number one can however probe deeper. We can correspondingly define

$$\lambda^\star(p, \mathrm{SNR}_k) = \frac{2\pi\alpha^\star(p, \mathrm{SNR}_k)}{p} , \tag{27}$$

which has the interpretation of being the resolution at the maximum probing depth. In Figures 3 and 4 respectively we show the resolving radius $\alpha^\star$ and the associated resolution $\lambda^\star$.

In fact, for large SNR_k, $p \mapsto \lambda^\star(p, \mathrm{SNR}_k)$ has a maximum. The argument at the extremal, $p^\star$, satisfies

$$p^\star(\mathrm{SNR}_k) \overset{\mathrm{SNR}_k \uparrow \infty}{\sim} \frac{1}{2} \ln(\mathrm{SNR}_k) .$$

We also have

$$\alpha^\star(p^\star(\mathrm{SNR}_k), \mathrm{SNR}_k) \overset{\mathrm{SNR}_k \uparrow \infty}{\sim} e^{-1} ,$$

which conforms with the behavior seen in Figure 2. We then have the following asymptotic characterization of the resolution:

$$\lambda^\star(p^\star(\mathrm{SNR}_k), \mathrm{SNR}_k) \overset{\mathrm{SNR}_k \uparrow \infty}{\sim} \frac{4\pi}{e \, \ln(\mathrm{SNR}_k)} .$$

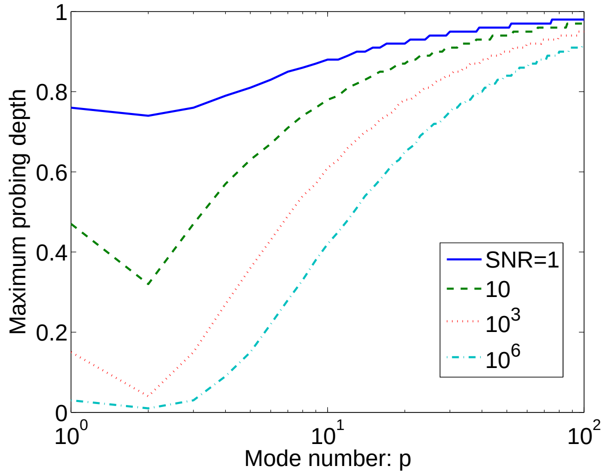

FIGURE 3. Resolving radius $\alpha^\star(p, \mathrm{SNR}_k)$ (see (26)) as function of mode number p and signal to noise ratio SNR_k.

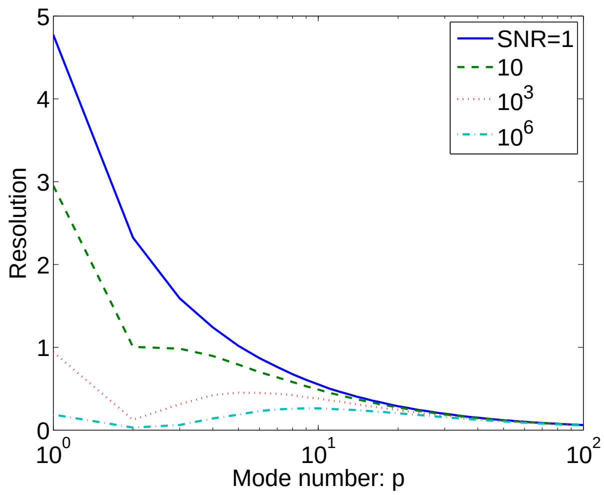

FIGURE 4. Resolution $\lambda^\star(p, \mathrm{SNR}_k)$ (see (27)) as function of mode number p and signal to noise ratio SNR_k.

We conclude that indeed the conductivity is sensitive to noise with a high resolution requiring a very high signal to noise ratio.

3. DETECTION WITH HELMHOLTZ DATA

We now change the focus to the wave propagation problem. That is, we consider the case when the data are time-harmonic observations, the solutions of the Helmholtz equation and we consider the analogous estimation problem as that discussed in the previous section.

3.1. **Differential Measurements.** The measurements are taken on a circle of unit radius in a non-dimensionalized setting. The domain of interest and the perturbation domain is as before characterized by (1) and (2). Following [3] we model the estimation problem below. Suppose first that the inclusion D_ε is illuminated by an array of N elements $\{\boldsymbol{y}_1, \dots, \boldsymbol{y}_N\}$. In polar coordinates the points of the transmitter array are $\boldsymbol{y}_n = (\cos\theta_n, \sin\theta_n)$. In this case, the field perturbed in the presence of the inclusion is the solution $u(\cdot, \boldsymbol{y}_m)$ to the following transmission problem:

$$
\begin{cases}
\Delta u + \dfrac{\omega^2}{c_0^2} u = -\delta_{\boldsymbol{y}_m}\,, & \text{in } \mathbb{R}^2 \setminus \overline{D_\varepsilon}\,,\\
\Delta u + \dfrac{\omega^2}{c^2} u = 0\,, & \text{in } D_\varepsilon\,,\\
u\big|_+ - u\big|_- = 0\,, & \text{on } \partial D_\varepsilon\,,\\
\dfrac{\partial u}{\partial \nu}\Big|_+ - \dfrac{\partial u}{\partial \nu}\Big|_- = 0\,, & \text{on } \partial D_\varepsilon\,,\\
u \text{ satisfies the outgoing radiation condition,}
\end{cases}
\tag{28}
$$

where ω/c_0 and ω/c are the wavenumbers associated with the free space and the inclusion respectively.

Suppose also that the receiver array used to detect the inclusion coincides with the transmitter array. The data consists of the multi-static response (MSR) matrix $\mathbf{A} = (A_{n,m})_{n,m=1,\dots,N}$ which describes the transmit-receive process performed by this array. In the presence of the inclusion the scattered field induced on the nth receiving element, $\boldsymbol{y}_n$, from the scattering of an incident wave generated at $\boldsymbol{y}_m$ can be expressed as follows:

$$
A_{n,m} = u(\boldsymbol{y}_n, \boldsymbol{y}_m) - \Gamma^{q_0}(\boldsymbol{y}_n - \boldsymbol{y}_m)\,. \tag{29}
$$

Here $q_0 = \omega/c_0$ is the homogeneous wavenumber, Γ^{q_0} is the associated free space Green's function:

$$
\Gamma^{q_0}(\boldsymbol{x}) = \frac{i}{4} H_0^{(1)}\big(q_0|\boldsymbol{x}|\big) \overset{q_0|\boldsymbol{x}|\gg 1}{\simeq} \frac{e^{i\pi/4}}{2\sqrt{2\pi q_0|\boldsymbol{x}|}} e^{iq_0|\boldsymbol{x}|}, \tag{30}
$$

and $H_0^{(1)}$ is the Hankel function of the first kind of order zero.

The problem we consider is to image the inclusion D from the MSR matrix. We assume that the target is extended, *i.e.*, its characteristic size is much larger than half the wavelength π/q_0.

Let us define the contrast parameter

$$
\mathcal{C} = \frac{c_0^2}{c^2} - 1\,. \tag{31}
$$

As shown in [3] (see also [16, 17, 23]) the response matrix is given asymptotically when $c \sim c_0$ by

$$
A_{m,n}[D] = \frac{iq_0\mathcal{C}}{8\pi} \int_D e^{iq_0[|\boldsymbol{y}_n - \boldsymbol{x}| + |\boldsymbol{y}_m - \boldsymbol{x}|]} d\boldsymbol{x}\,. \tag{32}
$$

Using the Taylor series expansion

$$
|\boldsymbol{y}_n - \boldsymbol{x}| = |\boldsymbol{y}_n| - \frac{\boldsymbol{y}_n \cdot \boldsymbol{x}}{|\boldsymbol{y}_n|} + O\Big(\frac{|\boldsymbol{x}|^2}{|\boldsymbol{y}_n|}\Big)\,, \tag{33}
$$

we find that, in polar coordinates $\boldsymbol{x} = (r\cos\theta, r\sin\theta)$,

$$A_{m,n}[D] = e^{i(2q_0+\pi/2)}\frac{q_0\mathcal{C}}{8\pi}\int_0^{2\pi} d\theta \int_0^{\alpha} rdr e^{-iq_0 r[\cos(\theta-\theta_m)+\cos(\theta-\theta_n)]}\,, \tag{34}$$

which is valid if $q_0 \mathrm{diam}^2(D)$ is smaller than the distance from the target D to the array (this is the Fraunhofer regime). Thus, we make the assumption

Assumption 2. $\alpha^2 q_0 \ll 1$.

Similarly, we have for the case of measurements from the perturbed domain

$$A_{m,n}[D_\varepsilon] = e^{i(2q_0+\pi/2)}\frac{q_0\mathcal{C}}{8\pi}\int_0^{2\pi} d\theta \int_0^{\alpha+\varepsilon h(\theta)} rdr e^{-iq_0 r[\cos(\theta-\theta_m)+\cos(\theta-\theta_n)]}\,. \tag{35}$$

Expansions (32) and (35) are known as the Born approximations.

In the continuum approximation the response matrix of the unperturbed domain then corresponds to the operator whose kernel is

$$\mathcal{A}[D](\theta_1,\theta_2) = \frac{q_0\mathcal{C}}{8\pi}\int_0^{2\pi} d\theta \int_0^{\alpha} rdr e^{-iq_0 r[\cos(\theta-\theta_1)+\cos(\theta-\theta_2)]}\,. \tag{36}$$

The kernel of the operator corresponding to the perturbed domain has a similar expression with $\alpha+\varepsilon h(\theta)$ instead of α. Therefore the kernel associated with differential measurements can be written as

$$\mathcal{H}[D](\theta_1,\theta_2) = \frac{q_0\mathcal{C}\alpha\varepsilon}{8\pi}\int_0^{2\pi} d\theta e^{-iq_0\alpha[\cos(\theta-\theta_1)+\cos(\theta-\theta_2)]}h(\theta)\,. \tag{37}$$

It is convenient to express the data in the continuum approximation and in the Fourier domain as the singular vectors of the kernel indeed constitute the Fourier basis. This moreover corresponds to the measurement configuration of the conductivity case discussed in the previous section. We then have the response matrix observations

$$\hat{b}_{n,m} = \frac{1}{(2\pi)^2}\int_0^{2\pi}\int_0^{2\pi} \mathcal{H}[D](\theta_1,\theta_2)e^{-i(n\theta_1+m\theta_2)}d\theta_1 d\theta_2\,, \tag{38}$$

and they are given by

$$\hat{b}_{n,m} = \frac{\varepsilon q_0\mathcal{C}\alpha}{4}J_n(q_0\alpha)J_m(q_0\alpha)i^{-(n+m)}\hat{h}_{n+m}\,, \tag{39}$$

where the J_n's are the Bessel functions of the first kind. The coefficients $\hat{b}_{n,m}$ are the analogue of $\hat{a}_{n,m}$ for the conductivity case. If we incorporate instrument noise and again assume that the effect of approximation error is relatively small, then we can write

$$\hat{b}^{\mathrm{meas}}_{n,m} = \hat{b}_{n,m} + \sigma\hat{W}_{n,m}\,, \tag{40}$$

with again $\hat{W}_{n,m}$ being modeled as standard and independent circularly symmetric Gaussian entries. The analogue of (9) then becomes

$$\hat{b}_{n,m} = (\mathcal{R}\hat{h})_{n,m}\,, \qquad (\mathcal{R}\hat{h})_{n,m} = \frac{\varepsilon q_0\mathcal{C}\alpha}{4}J_n(q_0\alpha)J_m(q_0\alpha)i^{-(n+m)}\hat{h}_{n+m}\,. \tag{41}$$

We then get the least squares estimate

$$
\begin{aligned}
\hat{h}_{\mathrm{est},p} &= \hat{h}_p + \sigma\big((\mathcal{R}^*\mathcal{R})^{-1}\mathcal{R}^*\hat{W}\big)_p \\
&= \hat{h}_p + \frac{4\sigma}{\varepsilon q_0 \mathcal{C}\alpha} \frac{\sum_{l=-\infty}^{\infty} J_l(q_0\alpha) J_{p-l}(q_0\alpha) i^p \hat{W}_{l,p-l}}{\sum_{l=-\infty}^{\infty} J_l^2(q_0\alpha) J_{p-l}^2(q_0\alpha)}, \qquad (42)
\end{aligned}
$$

which shows that the estimation is unbiased with the variance

$$
\begin{aligned}
\mathrm{Var}(\hat{h}_{\mathrm{est},p}) &= \mathbb{E}\Big[\big|\hat{h}_{\mathrm{est},p} - \hat{h}_p\big|^2\Big] = \Big(\frac{4\sigma}{\varepsilon q_0 \mathcal{C}\alpha}\Big)^2 \frac{1}{\sum_{l=-\infty}^{\infty} J_l^2(q_0\alpha) J_{p-l}^2(q_0\alpha)} \\
&= \Big(\frac{4\sigma}{\varepsilon q_0 \mathcal{C}\alpha}\Big)^2 \frac{2\pi}{\int_0^{2\pi} J_p^2(2q_0\alpha\cos\theta) d\theta}. \qquad (43)
\end{aligned}
$$

Here we have used of the formula

$$
\sum_{l=-\infty}^{\infty} J_l^2(q_0\alpha) J_{p-l}^2(q_0\alpha) = \frac{1}{2\pi}\int_0^{2\pi} J_p^2(2q_0\alpha\cos\theta) d\theta, \qquad (44)
$$

which follows from Neumann's formula [14, Formula 7.7.2(11)] and Parseval's formula.

We consider in the next two subsections the high- and low-frequency regimes.

3.2. **High-frequency regime.** We consider the high-frequency regime defined by:

Assumption 3. $q_0\alpha \gg 1$.

We remark that assumptions 2 and 3 imply $\alpha \ll 1$ and $q_0 \gg 1$. In this asymptotic framework, when p is smaller than $2q_0\alpha$, then we have [22, Eq. 4]

$$
\begin{aligned}
\frac{1}{2\pi}\int_0^{2\pi} J_p^2(2q_0\alpha\cos\theta) d\theta = \frac{1}{\pi^2 q_0\alpha}\Big[&\log q_0\alpha + 5\ln 2 + \gamma - 2\big(1 + \frac{1}{3} + \cdots + \frac{1}{2p-1}\big) \\
&+ O\big((q_0\alpha)^{-1/2}\big)\Big], \qquad (45)
\end{aligned}
$$

where γ is the Euler's constant, while when p is larger than $2q_0\alpha$, then the integral is exponentially close to zero [1, Eq. 9.3.2]:

$$
\frac{1}{2\pi}\int_0^{2\pi} J_p^2(2q_0\alpha\cos\theta) d\theta \sim \exp\Big[-4q_0\alpha R\big(\frac{p}{2q_0\alpha}\big)\Big], \qquad (46)
$$

with $R(s) = s\big[\cosh^{-1}(s) - \tanh\big(\cosh^{-1}(s)\big)\big]$ and $\cosh^{-1}$ is the inverse hyperbolic cosine.

We introduce the signal to noise ratio SNR and the contrast adjusted signal to noise ratio $\mathrm{SNR}_{\mathcal{C}}$:

$$
\mathrm{SNR} = \Big(\frac{\varepsilon}{\sigma}\Big)^2, \qquad \mathrm{SNR}_{\mathcal{C}} = \mathcal{C}^2 \mathrm{SNR}. \qquad (47)
$$

The stability condition that allows for the estimation of the pth mode is:

$$
\mathrm{Var}(\hat{h}_{\mathrm{est},p}) < 1, \qquad (48)
$$

with $\mathrm{Var}(\hat{h}_{\mathrm{est},p})$ given by (43). For $p < 2q_0\alpha$, this condition reads:

$$
\mathrm{SNR}_{\mathcal{C}}^{-1} < \frac{q_0\alpha \log(q_0\alpha)}{(4\pi)^2}. \qquad (49)
$$

For $p > 2q_0\alpha$ the condition (48) means that $\mathrm{SNR}_{\mathcal{C}}^{-1}$ should be exponentially large in $q_0\alpha$. Therefore we need $p < 2q_0\alpha$, otherwise the signal is exponentially small

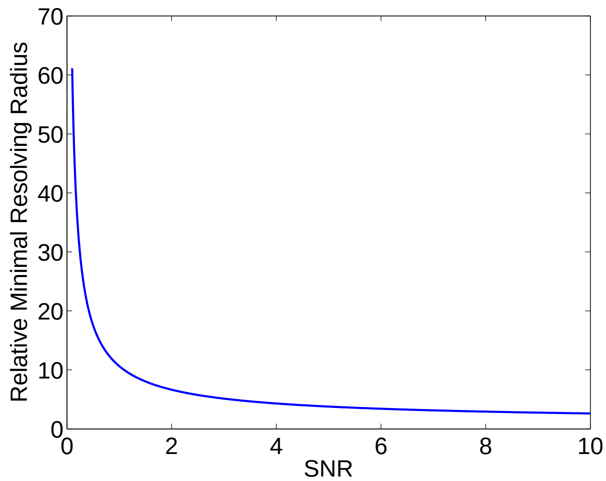

FIGURE 5. Relative minimal radius $\alpha^\star(\mathrm{SNR}_{\mathcal{C}})/\lambda_0$ (see (51)) as function of $\mathrm{SNR}_{\mathcal{C}}$ in the high-frequency regime.

and the constraint on the signal to noise ratio is prohibitive. This corresponds to the "global" resolution constraint:

$$p \leq p(\alpha)\,, \qquad \frac{2\pi\alpha}{p(\alpha)} = \frac{\lambda_0}{2}\,, \tag{50}$$

where $\lambda_0 = 2\pi/q_0$ is the homogeneous wavelength. Thus, this constraint limits the resolution to half the wavelength.

In order to estimate the coefficients $\hat{h}_p$ for all $p \leq 2q_0\alpha$ we need (49) to be satisfied. Note that a large parameter $q_0\alpha$ actually allows for the estimation of the coefficients $\hat{h}_p$ for a small $\mathrm{SNR}_{\mathcal{C}}$ since the high frequency q_0 amplifies the returns as shown in (37). This shows that in this high-frequency regime the estimation is relatively insensitive to noise. From (49) we have for the probing constraint

$$\alpha \geq \alpha^\star(\mathrm{SNR}_{\mathcal{C}})\,, \qquad \alpha^\star(\mathrm{SNR}_{\mathcal{C}}) = \frac{\lambda_0}{2\pi}\mathcal{F}^{-1}\left((4\pi)^2\mathrm{SNR}_{\mathcal{C}}^{-1}\right)\,. \tag{51}$$

where $\mathcal{F}(x) = x\log x$ is an increasing one-to-one function from $[1,\infty)$ to $[0,\infty)$. The radius $\alpha^\star$ is the minimal radius of the inclusion that can be probed and estimated with a signal to noise ratio $\mathrm{SNR}_{\mathcal{C}}$ in the high-frequency regime. In Figure 5 we show the relative minimal resolving radius $\alpha^\star/\lambda_0$ as function of $\mathrm{SNR}_{\mathcal{C}}$. We remark that Assumption 3 means that $2\pi\alpha/\lambda_0 \gg 1$.

3.3. **Low-frequency regime.**

We consider the low-frequency regime defined by:

Assumption 4. $q_0\alpha \ll 1$.

In the asymptotic framework when $q_0\alpha \ll 1$, using that $J_p(z) \overset{z\to 0}{\sim} (z/2)^p/p!$, we have

$$\frac{1}{2\pi}\int_0^{2\pi} J_p^2(2q_0\alpha\cos\theta)d\theta \sim (q_0\alpha)^{2p}\mathcal{H}(p)\,, \tag{52}$$

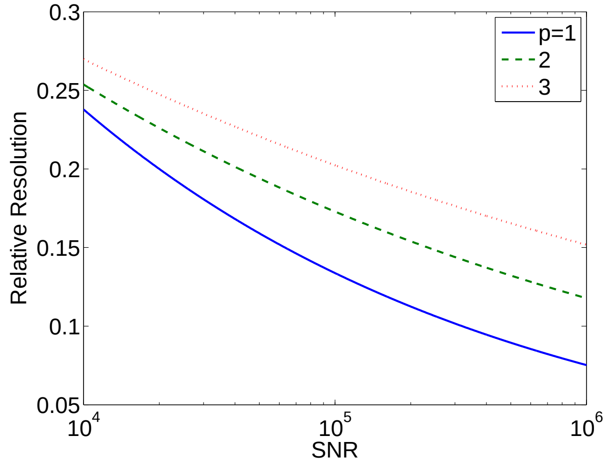

FIGURE 6. Maximal mode number $p(\alpha/\lambda_0, \mathrm{SNR}_\mathcal{C})$ (see (55)) as function of relative radius α/λ_0 and signal to noise ratio $\mathrm{SNR}_\mathcal{C}$ in the low-frequency regime.

with

$$\mathcal{H}(p) = \frac{1}{2\pi(p!)^2} \int_0^{2\pi} \cos^{2p}(\theta) d\theta = \frac{1}{4} \frac{(2p)!}{2^{2p}(p!)^4} . \tag{53}$$

We then get (as in (48)) the stability condition that allows for the estimation of the pth mode:

$$\mathrm{SNR}_\mathcal{C}^{-1} < \frac{(q_0\alpha)^{2p+2}\mathcal{H}(p)}{4} = \Big(\frac{2\pi\alpha}{\lambda_0}\Big)^{2p+2} \frac{\mathcal{H}(p)}{4} . \tag{54}$$

Note the qualitative different dependence on the mode number in the high- and low-frequency regimes (compare with (49)). We can now answer the question: for a fixed $\mathrm{SNR}_\mathcal{C}$ and α which modes can be resolved? The answer is that it is possible to estimate modes up to $p = p(\alpha/\lambda_0, \mathrm{SNR}_\mathcal{C})$ with

$$p(\alpha/\lambda_0, \mathrm{SNR}_\mathcal{C}) = \sup \Big\{ p \geq 1 \, \Big| \inf_{1 \leq p' \leq p} \Big(\frac{2\pi\alpha}{\lambda_0}\Big)^{2p'+2} \frac{\mathcal{H}(p')}{4} > \mathrm{SNR}_\mathcal{C}^{-1} \Big\} . \tag{55}$$

We plot in Figure 6 the maximal mode number $p(\alpha/\lambda_0, \mathrm{SNR}_\mathcal{C})$ as function of the relative radius α/λ_0 and signal to noise ratio $\mathrm{SNR}_\mathcal{C}$. We remark that Assumption 4 means that $2\pi\alpha/\lambda_0 \ll 1$. Note that a high signal to noise ratio is needed in this low-frequency regime even to get estimates of relatively low modes. Figure 7 shows the resolution bound as defined by (25):

$$\frac{\lambda(\alpha/\lambda_0, \mathrm{SNR}_\mathcal{C})}{\lambda_0} = 2\pi \frac{\alpha/\lambda_0}{p(\alpha/\lambda_0, \mathrm{SNR}_\mathcal{C})} , \tag{56}$$

with $p(\alpha/\lambda_0, \mathrm{SNR}_\mathcal{C})$ given by (55).

In terms of the radial dependence we can contrast (54) with the corresponding condition in (21). The low-frequency limit is very sensitive to the noise conforming with the discussion of the conductivity case in the previous section. From (54) we

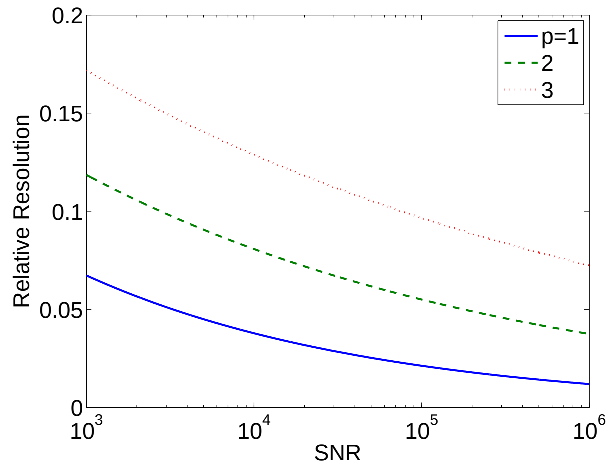

FIGURE 7. Relative resolution $\lambda(\alpha/\lambda_0, \mathrm{SNR}_{\mathcal{C}})/\lambda_0$ (see (56)) as function of relative radius α/λ_0 and signal to noise ratio $\mathrm{SNR}_{\mathcal{C}}$ in the low-frequency regime.

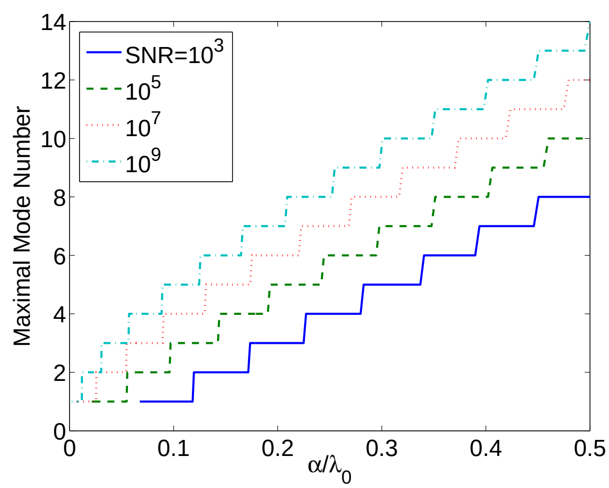

FIGURE 8. Relative minimal radius $\alpha^\star(p, \mathrm{SNR}_{\mathcal{C}})/\lambda_0$ (see (57)) as function of $\mathrm{SNR}_{\mathcal{C}}$ and mode number p in the low-frequency regime.

have the probing constraint

$$\alpha \geq \alpha^\star(p, \mathrm{SNR}_{\mathcal{C}}), \qquad \alpha^\star(p, \mathrm{SNR}_{\mathcal{C}}) = \frac{\lambda_0}{2\pi}\left(\frac{4}{\mathcal{H}(p)\mathrm{SNR}_{\mathcal{C}}}\right)^{1/(2p+2)}, \tag{57}$$

which is the low-frequency version of (51). This answers the question: for the mode number p that we want to resolve and a given signal to noise ratio $\mathrm{SNR}_{\mathcal{C}}$, what is the minimum radius $\alpha^\star$ that we can probe? We plot the relative minimal radius $\alpha^\star/\lambda_0$ in Figure 8.

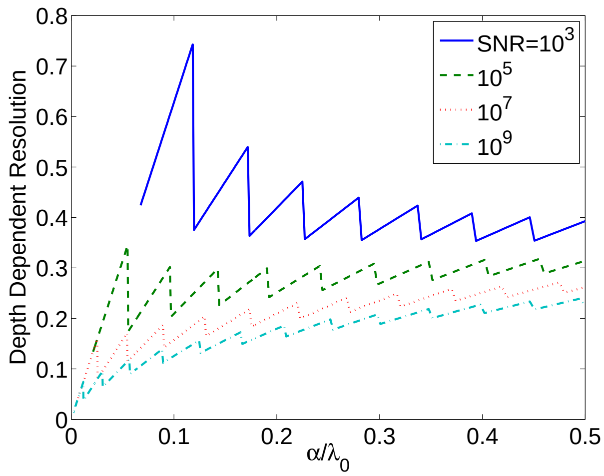

FIGURE 9. Relative resolution measure $\lambda^\star(p, \mathrm{SNR}_{\mathcal{C}})/\lambda_0$ (see (58)) as function of $\mathrm{SNR}_{\mathcal{C}}$ and mode number p in the low-frequency regime.

We can next associate the relative minimum radius with the resolution measure $\lambda^\star(p, \mathrm{SNR}_{\mathcal{C}}) = 2\pi\alpha^\star(p, \mathrm{SNR}_{\mathcal{C}})/p$. Thus, we introduce the p- and SNR-dependent resolution constraint by:

$$\lambda^\star(p, \mathrm{SNR}_{\mathcal{C}}) = \frac{\lambda_0}{p}\Big(\frac{4}{\mathcal{H}(p)\mathrm{SNR}_{\mathcal{C}}}\Big)^{1/(2p+2)}. \tag{58}$$

Using Stirling's formula, it follows from (58) that

$$\lambda^\star(p, \mathrm{SNR}_{\mathcal{C}}) \overset{p\to\infty}{\sim} \frac{\lambda_0}{e}. \tag{59}$$

We plot the resolution measure $\lambda^\star(p, \mathrm{SNR}_{\mathcal{C}})/\lambda_0$ in Figure 9. Note that this measure is very sensitive to the mode number and SNR in this low-frequency regime, a relatively high signal to noise ratio is needed. However, with a very high signal to noise ratio the relative resolution can then be very high.

REFERENCES

[1] M. Abramowitz and I. Stegun (editors), *Handbook of Mathematical Functions*, National Bureau of Standards, Washington D.C., 1964.

[2] H. Ammari, E. Beretta, E. Francini, H. Kang, and M. Lim, Reconstruction of small interface changes of an inclusion from modal measurements II: The elastic case, J. Math. Pures Appl., 94 (2010), 322–339.

[3] H. Ammari, J. Garnier, H. Kang, M. Lim, and K. Sølna, Multistatic imaging of extended targets, SIAM J. Imaging Science, 2011, to appear.

[4] H. Ammari, H. Kang, and H. Lee, *Layer Potential Techniques in Spectral Analysis*, Mathematical Surveys and Monographs, Vol. 153, Amer. Math. Soc., Providence RI, 2009.

[5] H. Ammari, H. Kang, M. Lim, and H. Zribi, Conductivity interface problems. Part I: Small perturbations of an interface, Trans. Amer. Math. Soc., 362 (2010), 2435–2449.

[6] G. Bao, Y. Chen, and F. Ma, Regularity and stability for the scattering map of a linearized inverse medium problem, J. Math. Anal. Appl., 247 (2000), 255–271.

[7] E. Beretta and E. Francini, Asymptotic formulas for perturbations in the electromagnetic fields due to the presence of thin inhomogeneities, in *Inverse problems: theory and applications*, Contemp. Math., 333, Amer. Math. Soc., Providence, RI, 2003.
[8] M. Bertero, P. Boccacci, and M. Piana, Resolution and super-resolution in inverse diffraction, in *Inverse Problems of Wave Propagation and Diffraction*, Lecture Notes in Physics, Vol. 486, 1–17, Springer, Berlin, 1997.
[9] L. Borcea, Electrical impedance tomography, Inverse Problems 18 (2002), R99–R136.
[10] L. Borcea, G. Papanicolaou, and F. G. Vasquez, Edge illumination and imaging of extended reflectors, SIAM J. Imaging Sci., 1 (2008), 75–114.
[11] D. C. Dobson, Estimates on resolution and stabilization for the linearized inverse conductivity problem, Inverse Problems 8 (1992), 71–81.
[12] D. C. Dobson and F. Santosa, Resolution and stability analysis of an inverse problem in electrical impedance tomography: dependence on the input current patterns, SIAM J. Appl. Math., 54 (1994), 1542–1560.
[13] G. Derveaux, G. Papanicolaou, and C. Tsogka, Resolution and denoising in near-field imaging, Inverse Problems, 22 (2006), 1437–1456,
[14] A. Erdélyi, W. Magnus, F. Oberhettinger, and F. G. Tricomi (editors), *Higher Transcendental Functions, Vol. II*, McGraw-Hill, New York, 1953.
[15] B. Harrach and J. K. Seo, Exact shape-reconstruction by one-step linearization in electrical impedance tomography, SIAM J. Math. Anal., 42 (2010), 1505–1518.
[16] S. Hou, K. Sølna, and H. Zhao, A direct imaging algorithm for extended targets, Inverse Problems, 22 (2006), 1151–1178.
[17] S. Hou, K. Sølna, and H. Zhao, Imaging of location and geometry for extended targets using the response matrix, J. Comput. Phys., 199 (2004), 317–338.
[18] D. Isaacson and E. L. Isaacson, Comment on A.-P. Calderón paper: "On an inverse boundary value problem", Math. Comp., 52 (1989), 553–559.
[19] V. Isakov, Increased stability in the Cauchy problem for some elliptic equations, in *Instability in Models Connected with Fluid Flows. I*, C. Bardos and A. Fursikov, eds., International Math. Series, Vol. 6, 339–362, Springer, 2008.
[20] S. Nagayasu, G. Uhlmann, and J.-N. Wang, Depth dependent stability estimates in electrical impedance tomography, Inverse Problems, 25 (2009), 075001.
[21] D. Slepian, Some comments on Fourier analysis, uncertainty and modeling, SIAM Review, 25 (1983), 379–393.
[22] R. Wong, Asymptotic expansion of $\int_0^{\pi/2} J_\nu^2(\lambda\cos\theta)d\theta$, Math. Comput., 50 (1988), 229–234.
[23] H. Zhao, Analysis of the response matrix for an extended target, SIAM J. Appl. Math., 64 (2004), 725–745.

Department of Mathematics and Applications, Ecole Normale Supérieure, 45 Rue d'Ulm, 75005 Paris, France.
E-mail address: habib.ammari@ens.fr

Laboratoire de Probabilités et Modèles Aléatoires & Laboratoire Jacques-Louis Lions, Université Paris VII, 75205 Paris Cedex 13, France.
E-mail address: garnier@math.jussieu.fr

Department of Mathematics, University of California, Irvine, CA 92697
E-mail address: ksolna@math.uci.edu